RSC Advances

PAPER

View Article Online
View Journal | View Issue

Cite this: *RSC Adv.*, 2017, **7**, 36755

Deciphering chemical bonding in $B_nH_n^{2-}$ ($n = 2$–17): flexible multicenter bonding

Yan-Fang Shen,[a] Chang Xu*[a] and Long-Jiu Cheng *[ab]

It is well known that *closo*-borane dianions $B_nH_n^{2-}$ are stable aromatic cages and possess $n + 1$ valence electron pairs, in accordance with Wade's rules. However, the electronic structures of *closo*-$B_nH_n^{2-}$ cannot be explained by a Lewis structure because of their electron-deficient character, while recent theoretical and experimental studies reveal that multicenter bonding is a key part in their electronic structures. In this work, flexible multicenter bonding of $B_nH_n^{2-}$ ($n = 2$–17) is studied using the adaptive natural density partitioning (AdNDP) method in order to get insight into their stability and aromaticity. The large HOMO–LUMO gaps and negative NICS values indicate their close-shell electronic structure. Further chemical bonding analysis shows that all $2n + 2$ delocalized valence electrons in *closo*-$B_nH_n^{2-}$ are involved in various delocalized σ and π multicenter bonding systems on their cage surface, well matched with different symmetric configurations. There are five types of multicenter bonds, including an open 3c–2e BBB bond, closed 3c–2e BBB bond, 4c–2e bond, 8c–2e bond and a fully delocalized bond, which are delocalized on a B_3 broken-line, B_3 triangle, B_4 rhombus, B_8 double-ring and the whole surface of the boron cage, respectively. Our work reveals the flexibility of multicenter bonding in diversified *closo*-$B_nH_n^{2-}$ clusters, giving new insights into the bonding nature of $B_nH_n^{2-}$.

Received 20th June 2017
Accepted 20th July 2017

DOI: 10.1039/c7ra06811e

rsc.li/rsc-advances

1. Introduction

The chemistry of boron is intriguing due to its electron-deficient character and delocalized bonding pattern. As a result, boron based clusters have rich forms of nanostructures, including quasi-planar, ring, two-dimensional sheet and cage.[1–22] Over the past decade, small boron clusters have been systematically characterized both experimentally and theoretically to exhibit planar or quasi-planar structures in their ground states except for B_{14}, but undergo the 2D-3D transition at B_{20} for neutral, at B_{27}^- for anionic and at B_{16}^+ for cationic clusters.[5,23–29] The double-ring tubular B_{20} is confirmed to be stable and aromatic.[30–32] The B_{40} cage is the first all-boron fullerene composed of hexagons and heptagons, according to the theoretical and experimental observation by photoelectron spectroscopy.[33] In addition, there are also many fascinating sandwich-type complexes, metalloborospherenes, metal-centered boron molecular wheels and drums by doping metallic elements in boron clusters.[25,34–49] Chemical bonding analyses reveal that there is numerous flexible multicenter bonding in the electronic structures of all these clusters.

The polyhedral *closo*-borane $B_nH_n^{2-}$ clusters have attracted much interest from theoretical and experimental chemists since their synthesis in the early 20th century,[50–58] especially for their bonding patterns. Lipscomb pointed out that the 3c–2e hydrogen bridge bond is the key part in the electronic structure of borane clusters, which was proved by experimental study. In 1971, Wade's rules gave the insight into topologic structures of deltahedral $B_nH_n^{2-}$ clusters. It revealed that there are $(n + 1)$ electron pairs delocalized on their *closo* cage surface, where n is the number of vertexes.[59] Mingos extended this principle to electron rich clusters to become popularly known as the Wade–Mingos rules.[60,61] In 1977, King and co-workers investigated the three-dimensional aromaticity in $B_nH_n^{2-}$ using algebraic graph-theoretical methods, providing the theoretical basis for the stability of these clusters.[62] Whereafter, O'Neill and Wade tried to apply the Kekulé-type structures which using chemical bonding instead of the delocalized structures to *closo*-borane dianions for suggesting the existence of 3c–2e bonds.[63,64] In 2011, Lentz group obtained crystal structures of $B_{10}H_{10}^{2-}$ and $B_{12}H_{12}^{2-}$, and revealed that both of them have 3c–2e bonds by electron density and atoms-in-molecules (AIM) analysis.[65]

Previous study reveals the structures and stability of *closo*-borane $B_nH_n^{2-}$ from their topologic structures according to Wade's rules, rather than in the view of chemical bonding. However, the chemical bonding pattern in the series of *closo*-borane $B_nH_n^{2-}$ has not been studied yet. As multicenter bonding is a popular language in the community of chemistry which is wildly used to interpret the electronic structure, stability and aromaticity of boron clusters, in this paper we try to reveal the nature of electronic structure in borane dianions $B_nH_n^{2-}$ ($n = 2$–17) series from this way.

[a]*Department of Chemistry, Anhui University, Hefei, Anhui 230601, P. R. China. E-mail: clj@ustc.edu; xuchang_1986@hotmail.com; Fax: +86-0551-63861435; Tel: +86-0551-63861435*

[b]*Anhui Province Key Laboratory of Chemistry for Inorganic/Organic Hybrid Functionalized Materials, Hefei, Anhui, 230601, P. R. China*

2. Computational methods

In this article, the geometrical structures of borane dianions $B_nH_n^{2-}$ (n = 2–17) are optimized using TPSSh functional which has been proved to be reliable in the study of boron clusters.[66–70] The optimization and the calculations of the nucleus-independent chemical shifts (NICS)[71] are performed at the TPSSh/6-311+G* level, the HOMO–LUMO gaps are estimated using time-dependent density-functional theory (TD-DFT) method. NICS value is a popular measurement for aromaticity, where negative value indicates aromaticity, and positive value implies antiaromaticity. The vibrational frequencies are also checked to confirm the stability of structures at the same level of theory. All the DFT calculations are carried out in GAUSSIAN 09 package.[72] Chemical bonding analysis are performed using the adaptive natural density partitioning (AdNDP) method.[73] The AdNDP analysis is an effective tool developed by Boldyrev's group for deciphering the nature of the localized and delocalized bonds in boron clusters.[14,74–76] Since the size of basis sets does not affect much of the AdNDP calculations, the 3-21G basis set is employed. Noncovalent interaction (NCI)[77] are plotted using Multiwfn[78] and VMD packages.[79] The visualization of the AdNDP results are realized using the MOLEKEL 5.4.0.8 program.[80]

3. Results and discussion

3.1 Geometries and stability

The borane dianions $B_nH_n^{2-}$ (n = 2–17) series are optimized at TPSSh/6-311+G* level. The $B_nH_n^{2-}$ (n = 6–12) and (n = 4, 5, 13–17) have been observed experimentally and investigated theoretically, respectively.[51–55,81,82] In order to grasp the structural features and assure the integrity in this family, $B_nH_n^{2-}$ with n = 2 and 3 are considered as well. The structures of borane dianions are taken from the previous studies of Lipscomb, Schleyer, Dreuw, and their co-workers.[50,81,82] Fig. 1 plots the geometric structures of $B_nH_n^{2-}$ (n = 2–17). $B_2H_2^{2-}$ and $B_3H_3^{2-}$ are isovalent to C_2H_2 and $C_3H_3^+$, as we expected, they possess alike linear and planar structures, respectively. $B_4H_4^{2-}$ is neither planar nor tetrahedral, but somewhere in between, exhibiting a D_{2d}-symmetric geometry. Borane dianions $B_nH_n^{2-}$ (n = 5–17) start to favor *closo*-structures with increasing cluster size, including n + 1 electron pairs, in accordance with Wade's rules. The smallest member of *closo*-borane family that has been synthesized is $B_6H_6^{2-}$, of which calculated bond length is 1.740 Å close to the experimental value (1.700 Å).[83]

To investigate the stability of $B_nH_n^{2-}$ series, the HOMO–LUMO energy gaps (E_{HL}) are computed using TPSSH/6-311+G* level. As shown in Fig. 2a, the HOMO–LUMO energy gaps at $n \leq 4$ are lower than ones at $n \geq 5$, the reason is supposed be that the structures are open-shaped at $n \leq 4$, but getting closed at $n \geq 5$. Moreover, for $B_nH_n^{2-}$ ($n \geq 5$), there are four valleys at n = 8, 11, 13, 15, probably due to the lower symmetry of clusters comparing with other borane dianions. The relative stability of the system is further evaluated with the second-order difference in the total energies (Δ^2E), which can be defined as: $\Delta^2E(B_nH_n^{2-}) = E(B_{n-1}H_{n-1}^{2-}) + E(B_{n+1}H_{n+1}^{2-}) - 2E(B_nH_n^{2-})$, where $E(B_{n-1}H_{n-1}^{2-})$, $E(B_{n+1}H_{n+1}^{2-})$, $E(B_nH_n^{2-})$ are total energies of the clusters $B_{n-1}H_{n-1}^{2-}$, $B_{n+1}H_{n+1}^{2-}$, $B_nH_n^{2-}$. The second-order difference in energies is previously applied to study the relative stability of other boron clusters, and in its curves, positive peaks correspond to more relatively stable structures.[84,85] The Δ^2E plot in Fig. 2b shows that, four peaks present at $B_6H_6^{2-}$, $B_{10}H_{10}^{2-}$, $B_{12}H_{12}^{2-}$, $B_{14}H_{14}^{2-}$, suggesting their higher relative stability than their neighbours. In addition, it can be found that, each positive Δ^2E value in Fig. 2b can correspond to a peak in Fig. 2a, the highest Δ^2E and E_{HL} value is found for $B_{12}H_{12}^{2-}$, indicating the highest one in the series of dianions considered.

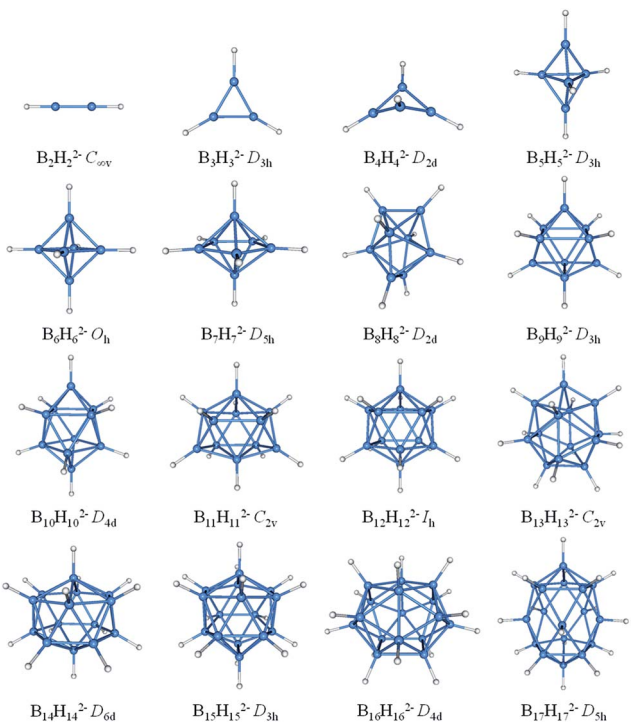

Fig. 1 Optimized geometries for borane dianions $B_nH_n^{2-}$ (n = 2–17) at TPSSH/6-311+G* level of theory. B-blue; H-white.

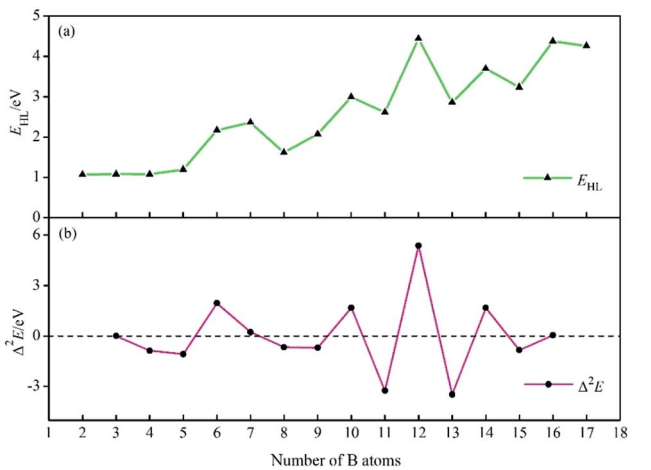

Fig. 2 HOMO–LUMO energy gaps E_{HL} (a) and the second-order differences in energy Δ^2E (b) of $B_nH_n^{2-}$ (n = 2–17).

3.2 Chemical bonding patterns

The theoretical study in 1963, Lipscomb's topological model involving *styx* numbers and rules inferred that *closo*-$B_nH_n^{2-}$ had $(n-2)$ 3c–2e BBB bonds and three 2c–2e BB bonds, which was somewhat limited in applicability.[50,86] Until today, the bonding nature of *closo*-$B_nH_n^{2-}$ is still one of the many intrigued mysteries in chemistry because of their complicated structure and electron deficiency. Apart from theoretical calculations of geometries, energies and aromaticity for *closo*-borane, no attempt to characterize chemical bonding in this family by means of AdNDP method has been carried out. Herein, chemical bonding analysis by AdNDP gives a more straightforward evidence for the multicenter bonding in $B_nH_n^{2-}$ ($n = 2$–17). The AdNDP method is wildly applied for closed-shell species recovering both the classical Lewis bonding concepts (lone-pairs and 2c–2e bonds) and the delocalized *n*c–2e bonds.

As shown in Fig. 3, B–B bond lengths in $B_2H_2^{2-}$ is 1.507 Å somewhat longer than a typical B≡B bond, while the B–B distance in $B_3H_3^{2-}$ is 1.634 Å between single B–B and double B=B bonds. In contrast with the previously reported C_2H_2 and $C_3H_3^+$ both geometries and bonds are similar for $B_2H_2^{2-}$ and $B_3H_3^{2-}$, respectively.[87] Then, we succeed in finding all expected multicenter bonds in these two clusters. For $B_2H_2^{2-}$, there are two 2c–2e σ-BH bonds and three 2c–2e BB bonds (B≡B triple bonds, including one σ and two π bonds) with occupy number (ON) 1.99|*e*|, 2.00|*e*|, respectively. In $B_3H_3^{2-}$, there are three 2c–2e σ-BH bonds, three 2c–2e σ-BB bonds and one delocalized 3c–2e π-BBB bond (ON = 2.00|*e*|, 1.95|*e*| and 2.00|*e*|, respectively). Similarly, $B_4H_4^{2-}$ has 10 valence electrons, featuring four 2c–2e σ-BH bonds, four 2c–2e σ-BB bonds and one 4c–2e delocalized over four boron atoms π-bond. Thus, bonding systems in boron framework of $B_3H_3^{2-}$ and $B_4H_4^{2-}$ are π-aromatic (2 electrons on one delocalized π-bond). $B_5H_5^{2-}$ is the least stable member in *closo*-$B_nH_n^{2-}$ and has never been synthesized. It has a three-membered ring with two caps in D_{3h} symmetry, the equatorial bonds are 1.827 Å and the axial bonds are 1.687 Å. Besides five 2c–2e σ-BH bonds, AdNDP analysis gives two bonding patters of the remained electrons of $B_5H_5^{2-}$. Pattern I includes three 3c–2e boron bridge σ bonds in the vertical direction and three delocalized 4c–2e σ bonds. Note that the open 3c–2e σ-BBB bond is formed by two apical B atoms and one of equatorial B atoms, while the apical B atom provides half of electron and the equatorial B atom provides one electron, respectively, such boron bridge bond was only observed previously in neutral borane (such as $B_{10}H_{14}$).[50] Pattern II includes six 3c–2e σ-BBB bonds on six triangles with ON = 1.90|*e*| which is smaller than the open one. Thus, we think pattern I is more reasonable.

The results of AdNDP analysis of $B_nH_n^{2-}$ ($n = 6$–8) are plotted in Fig. 4. $B_6H_6^{2-}$ is octahedral resonance structure, two bonding patterns are given in consideration of resonance effect. Pattern I includes six 2c–2e σ-BH bonds, six 3c–2e σ-BBB bonds and one delocalized 6c–2e σ bond, which is selected one of three-fold axis as main axis on account of the resonance effect. From pattern II, these 6c–2e orbitals can be clearly viewed as super S, $P_{x,y,z}$ and $D_{xy,yz,xz}$ orbitals. According to the spherical Jellium model,[88] 18-electron is the most stable magic number ($S^2P^6D^{10}$). The five D orbitals split into two sets in the octahedral field, and energy level of the double-degenerate orbital (D_{z^2} and $D_{x^2-y^2}$) increase due to the repulsion of BH bonds. Thus, 14-electron becomes stable magic number. For D_{5h} $B_7H_7^{2-}$, the equatorial bonds are 1.663 Å indeed smaller than the axial bonds (1.829 Å),

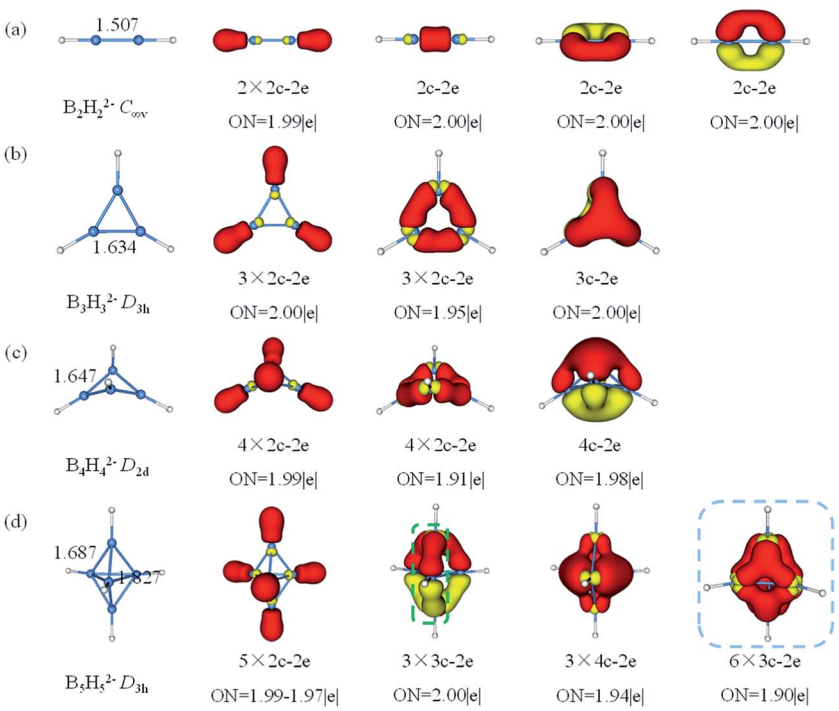

Fig. 3 Structures and AdNDP localized natural bonding orbitals of borane dianions. (a) $B_2H_2^{2-}$ (b) $B_3H_3^{2-}$ (c) $B_4H_4^{2-}$ (d) $B_5H_5^{2-}$. B-blue; H-white.

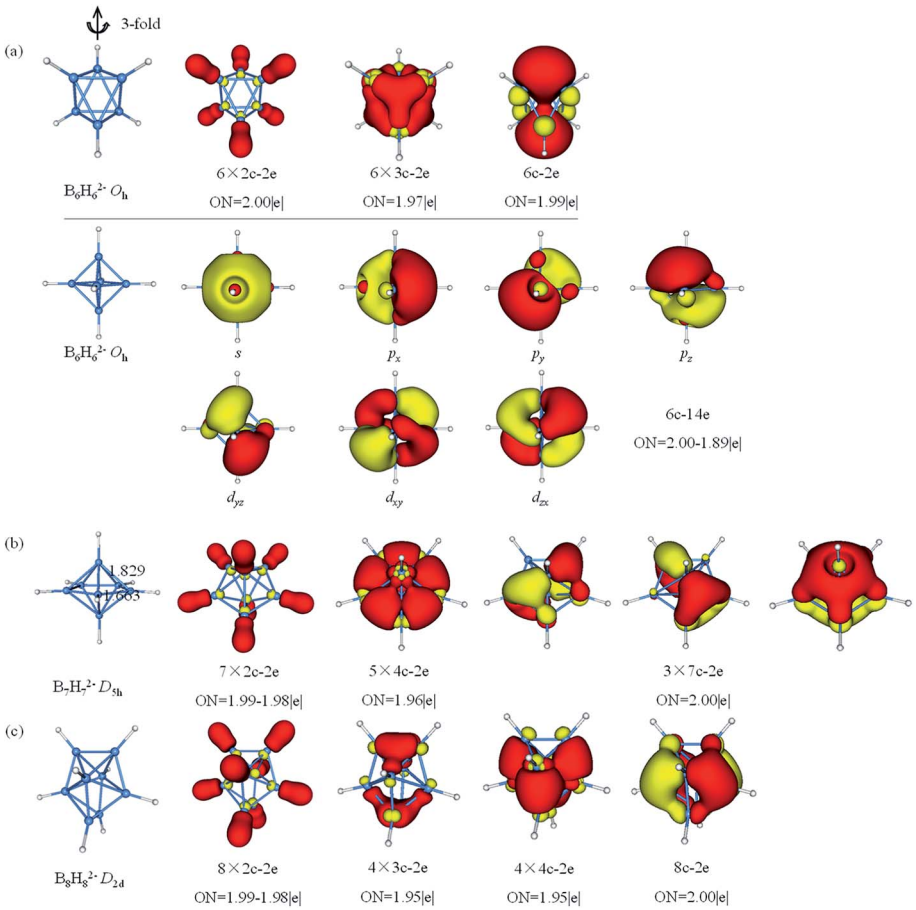

Fig. 4 Structures and AdNDP localized natural bonding orbitals of borane dianions. (a) $B_6H_6^{2-}$ (b) $B_7H_7^{2-}$ (c) $B_8H_8^{2-}$. B-blue; H-white.

which is prone to form 4c–2e bond. The σ-bonding framework includes seven 2c–2e σ-BH bonds and five delocalized 4c–2e σ bonds, the π-bonding framework consists of three delocalized 7c–2e π bonds. This type of π-bonding framework of $B_7H_7^{2-}$ is analogous to that of benzene. The bonding in $B_8H_8^{2-}$ can be explained by the formation of eight 2c–2e σ-BH bonds, four 3c–2e σ bonds, four 4c–2e σ bonds and one delocalized 8c–2e π bonds.

The AdNDP analysis of $B_nH_n^{2-}$ ($n = 9$–11) are shown in Fig. 5. The $B_9H_9^{2-}$ has a D_{3h} symmetry which can be divided into three layers (each layer has three B atoms). The AdNDP results reveal that there are 2c–2e σ-BH bonds, six 3c–2e σ bonds and four delocalized 9c–2e bonds. The six 3c–2e σ-BBB bonds are formed by six triangular lattices of middle layer B atoms bonding with top and bottom B_3 triangles. The four 9c–2e delocalized bonds can be classified into two sets including three 9c–2e delocalized π bonds and one 9c–2e delocalized σ bond, giving rise to double aromaticity (the delocalized π-system has 6 electrons following the $(4n + 2)$ rule for π-aromaticity and similarly for the delocalized σ-system). $B_{10}H_{10}^{2-}$ is square anti-prism geometry with two caps in D_{4d} symmetry. Three different distances of two B atoms are given in Fig. 5b, the bond lengths of two equatorial B atoms in (1.837 Å) or between (1.820 Å) two four-membered rings are clearly longer than the B–B distance (1.708 Å) between apical and equatorial B atoms. Thus, we guess that there are multicenter bonds in B_8 "double-ring". The AdNDP analysis reveals ten 2c–2e σ-BH bonds, eight 3c–2e σ-BBB bonds and three delocalized 8c–2e σ bonds, leading to σ-aromaticity. There are 46 valence electrons altogether in $B_{11}H_{11}^{2-}$ with C_{2v} symmetry. The results of the AdNDP analysis include eleven 2c–2e σ-BH bonds and twelve 3c–2e σ-BBB bonds with occupation numbers ranging from 1.77–1.92$|e|$.

The AdNDP analysis of $B_nH_n^{2-}$ ($n = 12$–14) are displayed in Fig. 6. The icosahedral $B_{12}H_{12}^{2-}$ cluster is the most stable molecule among polyhedral boranes observed experimentally up to now.[52,89,90] All of B atoms in I_h $B_{12}H_{12}^{2-}$ are equivalent, therefore, it can be treated for AdNDP analysis in similar way as $B_6H_6^{2-}$. Pattern I includes twelve 2c–2e σ-BH bonds, six 3c–2e σ-BBB bonds, six 4c–2e σ bonds and one delocalized 12c–2e bond. From pattern II, these orbitals are fulfilled with 26 valence electrons ($S^2P^6D^{10}F^8$), the $B_{12}H_{12}^{2-}$ possesses thirteen 12c–2e bonds and forms the closed-shell spherical structure. Similarly, seven F orbitals split into two sets in an icosahedral field, and only the lower quadruple-degenerate orbitals are filled. Both $B_{13}H_{13}^{2-}$ and $B_{11}H_{11}^{2-}$ are in lowest symmetry and have a relatively simple bonding pattern in this family. The $B_{13}H_{13}^{2-}$ dianion has 54 valence electrons that form thirteen 2c–2e σ-BH bonds and fourteen delocalized 3c–2e σ-BBB bonds distributing

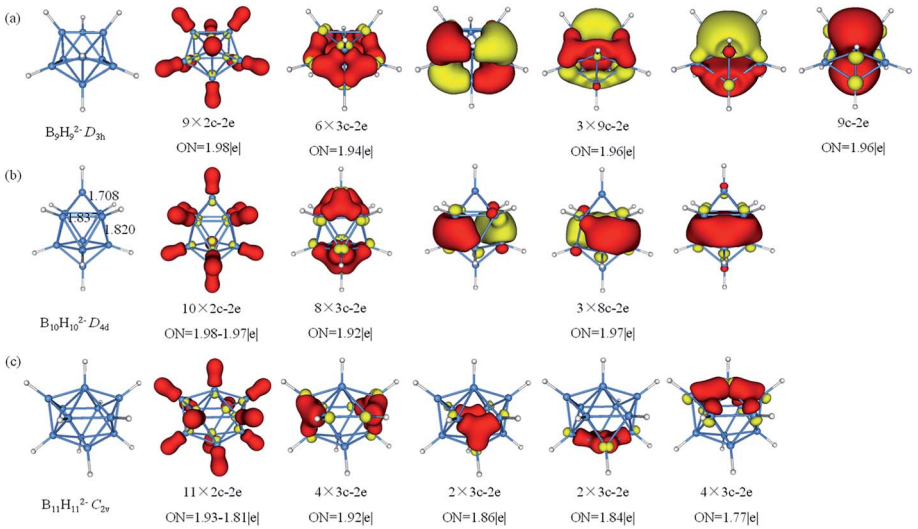

Fig. 5 Structures and AdNDP localized natural bonding orbitals of borane dianions. (a) $B_9H_9^{2-}$ (b) $B_{10}H_{10}^{2-}$ (c) $B_{11}H_{11}^{2-}$. B-blue; H-white.

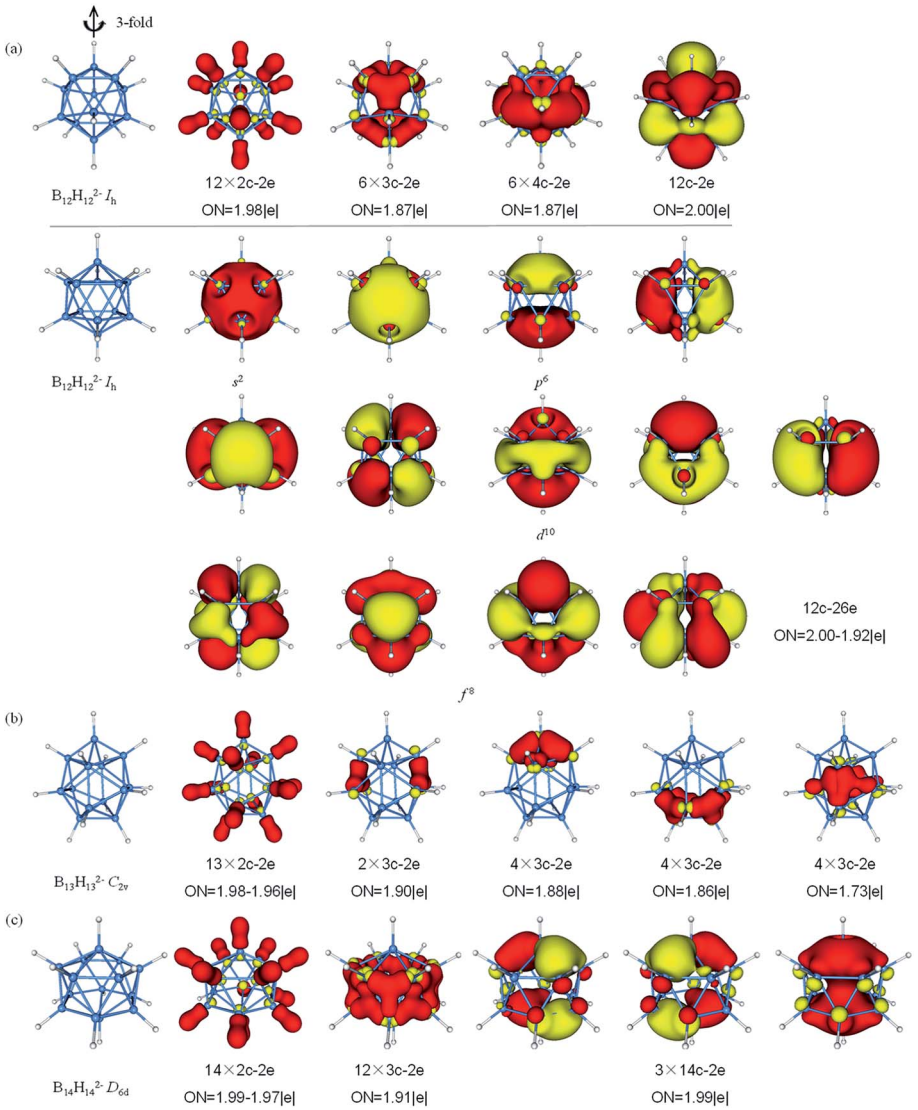

Fig. 6 Structures and AdNDP localized natural bonding orbitals of borane dianions. (a) $B_{12}H_{12}^{2-}$ (b) $B_{13}H_{13}^{2-}$ (c) $B_{14}H_{14}^{2-}$. B-blue; H-white.

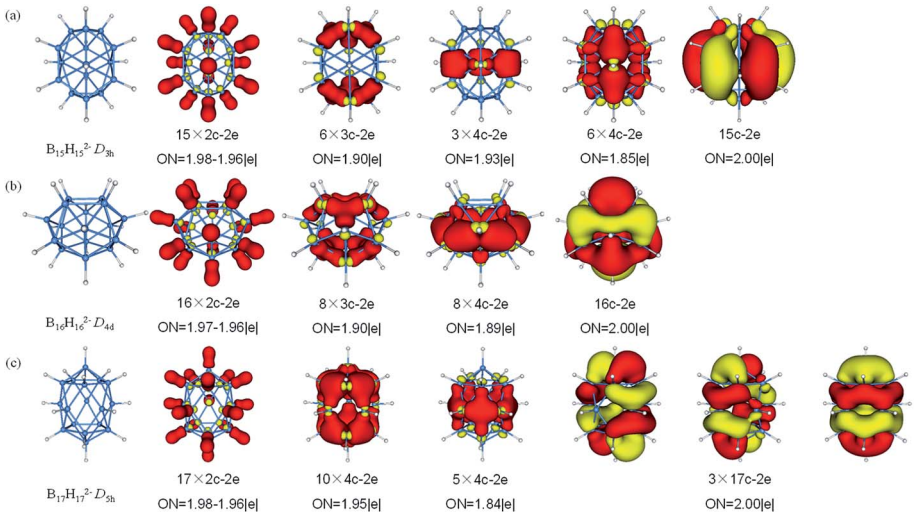

Fig. 7 Structures and AdNDP localized natural bonding orbitals of borane dianions. (a) $B_{15}H_{15}^{2-}$ (b) $B_{16}H_{16}^{2-}$ (c) $B_{17}H_{17}^{2-}$. B-blue; H-white.

on the left and right, top and bottom, front and back, in an overall symmetry of C_{2v}. $B_{14}H_{14}^{2-}$ is composed of two six-membered rings and two caps with D_{6d} symmetry. In contrast to the bond lengths in $B_{10}H_{10}^{2-}$, $B_{14}H_{14}^{2-}$ tends to bond between two six-membered rings. $B_{14}H_{14}^{2-}$ possesses fourteen 2c–2e σ-BH bonds, twelve 3c–2e σ-BBB bonds on twelve B_3 triangles forming a "double-ring", and three delocalized 14c–2e delocalized σ bonds, making the contribution to the σ-aromaticity of $B_{14}H_{14}^{2-}$.

The fifteen B atoms of D_{5h} $B_{15}H_{15}^{2-}$ can be classified into five three-membered rings of which can be available for bonding. There are 62 valence electrons in $B_{15}H_{15}^{2-}$, AdNDP analysis (Fig. 7) yields fifteen 2c–2e σ-BH bonds involving all atoms, six 3c–2e σ-BBB bonds which are shared by six B_3 triangles, three delocalized 4c–2e σ bonds around the middle of cage, six delocalized 4c–2e σ bonds covering on surface and one delocalized 15c–2e bond. The D_{4d} $B_{16}H_{16}^{2-}$ features a similar bonding pattern of $B_{12}H_{12}^{2-}$, with sixteen 2c–2e σ-BH bonds, eight 3c–2e σ-BBB bonds, eight delocalized 4c–2e σ bonds (are in a cycle just like a lantern) and one delocalized 16c–2e bond. $B_{17}H_{17}^{2-}$ is regard as "a hot candidate" for synthesis due to its high stability, aromaticity and symmetry through the theoretical study.[81] The 70 valence electrons in $B_{17}H_{17}^{2-}$ can be divided into three sets. The first set consists of localized bonding elements, seventeen 2c–2e σ-BH bonds, while the other two sets are composed of delocalized bonding elements, fifteen 4c–2e σ bonds (on the top, around the waist and at the bottom) and three 17c–2e delocalized bonds. The delocalized bonding can be viewed as three concentric σ-systems and one π-system, satisfying the $(4n + 2)$ rule for aromaticity, the similar delocalized bonding has been investigated in planar B_{13}^{+} which has two concentric σ-systems and one π-system.[91]

3.3 Aromaticity

From all above, it is believed that borane dianions with cage structure are highly stable from their relative energies. The stability and aromaticity can also be analyzed with the aid of a noncovalent interaction (NCI) method. The NCI index is based on the electron density (ρ) and the reduced density gradient (RDG, $s = 1/[2(3\pi^2)^{1/3}]|\nabla\rho|/\rho^{4/3}$), which can indicate the presence of noncovalent interactions with low-s low-ρ and covalent bonds with low-s high-ρ. The second ingredient of the NCI index adopts the second density Hessian eigenvalue (λ_2) to distinguish between bonding interactions ($\lambda_2 < 0$) and non-bonding interactions ($\lambda_2 > 0$). We believe that the NCI characteristic peak with disparate values of borane cage depends on their bonding patterns and all delocalized valence electrons distribute on the cage surface.

Fig. 8 plots the reduced density gradient (s) *versus* electron density (ρ) multiplied by the sign of λ_2 and the low-gradient ($s = 0.10$) NCI isosurfaces of the cage structure $B_{12}H_{12}^{2-}$ and $B_{10}H_{10}^{2-}$. As is illustrated in Fig. 8a, the high density, low-gradient spikes lie at about sign (λ_2) $\rho = -0.160$ and -0.126 a.u. for $B_{12}H_{12}^{2-}$, which represent strong covalent attractions. The more negative spike is clearly associated to the B–H covalent bonds which can be seen from NCI isosurfaces in the right part of Fig. 8, whereas the other strong attractive spike is the strong covalent interaction between boron atoms, indicating high stability and σ delocalization of $B_{12}H_{12}^{2-}$ cage. Similarly, there are one attractive spike (-0.160 a.u.) and the other two attractive spike (-0.136 and -0.108 a.u.) associated to the B–H covalent bonds and strong covalent interaction between boron atoms for $B_{10}H_{10}^{2-}$, which correspond to the blue regions of isosurfaces at the top (or bottom) and in the middle, respectively. Moreover, for $B_{12}H_{12}^{2-}$ and $B_{10}H_{10}^{2-}$, there are positive spikes at sign (λ_2) $\rho = 0.119$ and 0.103 a.u., respectively, which represent steric interactions among the boron atoms with the red regions of the isosurfaces. The results in Fig. 8 reveal that the spikes of B–H covalent interactions lie at about sign (λ_2) $\rho = -0.160$, and the rest of negative spikes with more intensive dots are because all the skeletal bonding electrons (in Wade's rules) of $B_{10}H_{10}^{2-}$ and $B_{12}H_{12}^{2-}$ are delocalized on the cage surface causing high stability. In addition, the number of NCI characteristic peak with negative values of $B_{10}H_{10}^{2-}$ is one more than

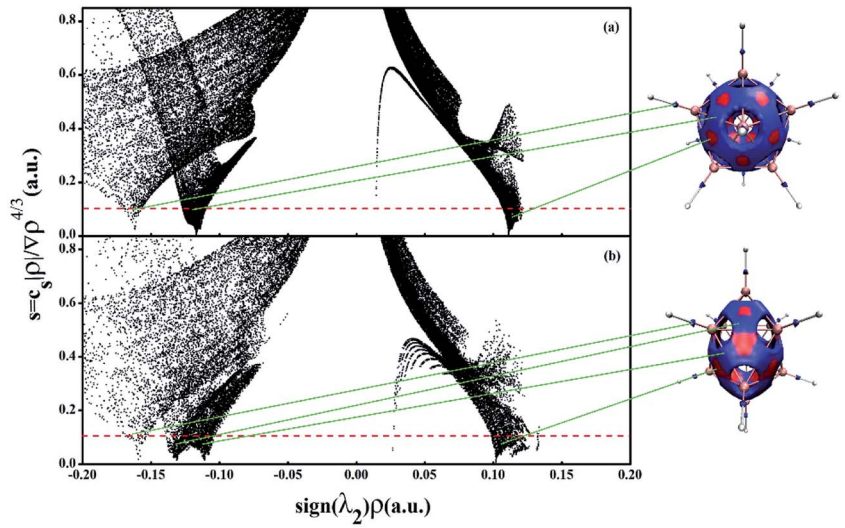

Fig. 8 Plots of the reduced density gradient *versus* the electron density multiplied by the sign of the second Hessian eigenvalue sign (λ_2) (left) and NCI isosurfaces using a blue-green-red color scale at $s = 0.10$ for $B_{12}H_{12}^{2-}$ (a) and $B_{10}H_{10}^{2-}$ (b), respectively.

that of $B_{12}H_{12}^{2-}$, which is due to the two different kinds of boron atoms in the former one, whereas the boron atoms of $B_{12}H_{12}^{2-}$ are equivalent.

In 2016, Poater and coworkers applied Hückel $(4n + 2)$ rule and Wade's rules in *closo*-$B_nH_n^{2-}$ to establish a connection between three-dimensional aromatic *closo* boron hydride clusters and planar aromatic annulenes.[92] Herein, NCI is a direct evidence to identify the aromaticity of clusters, and the aromatic characteristic of $B_nH_n^{2-}$ can obtain from their NICS value and electronic structures. We calculate the NICS values of above dianions except $B_2H_2^{2-}$ out of consideration for its line structure. As shown in Fig. 9, the negative NICS values suggest that all structures are aromatic. It should be noted that the tendency is accordant with E_{HL} gaps and NICS values (one wanes and the other one waxes), which indicates their close-shell electronic structures. For $B_3H_3^{2-}$ and $B_4H_4^{2-}$, both of them have two π electrons obeying $(4n + 2)$ Hückel rule with π-aromaticity. $B_nH_n^{2-}$ with $n = 5$–17 possess large negative NICS values from -17.91 to -29.13 ppm as a comparison with that of benzene of -11.92 ppm. $B_5H_5^{2-}$ is a watershed of structure and property in this system, which includes two categories of six delocalized σ electrons causing double σ-aromaticity in vertical and vertical direction, respectively. The O_h $B_6H_6^{2-}$ and I_h $B_{12}H_{12}^{2-}$ have two delocalized σ electrons along their five and ten 3-fold axis of symmetry as a consequence of resonance, respectively, showing large negative NICS values and E_{HL} gaps, which display high stability and strong aromaticity. The D_{5h} $B_7H_7^{2-}$ has ten σ and six π delocalized electrons leading to $(\sigma + \pi)$ aromaticity. $B_8H_8^{2-}$ is less stable with lower E_{HL} gap and smaller negative NICS value in the lower D_{2d} symmetry, the reason is probably that, there are two π and sixteen σ delocalized electrons, rendering π-aromaticity and σ-antiaromatic in $B_8H_8^{2-}$, according to the $(4n + 2)$ rule for aromaticity and $4n$ rule for antiaromaticity, respectively, but finally the former is dominated and counteract the latter. Likewise, $B_9H_9^{2-}$ and $B_{10}H_{10}^{2-}$ are $(\sigma + \pi)$ aromaticity and σ-aromaticity with $6\pi_{delo}$–$2\sigma_{delo}$ (six π delocalized and two σ delocalized) and $2\sigma_{delo}$ electrons, respectively. Both $B_{11}H_{11}^{2-}$ and $B_{13}H_{13}^{2-}$ have lower E_{HL} gaps and smaller negative NICS values than their neighbors, which perhaps on account of their lower symmetry, but are aromatic with close-shell electronic structures. The aromaticity of $B_{14}H_{14}^{2-}$ derives from its six delocalized σ electrons. The delocalized electrons of $B_{15}H_{15}^{2-}$ can be segmented into six parts, which include $5 \times 6\sigma_{delo}$ electrons from top to bottom and $2\sigma_{delo}$ electrons around whole structure, according to Hückel rule. The result of $B_{16}H_{16}^{2-}$ is similar to that of $B_8H_8^{2-}$, but allowing higher aromaticity with higher symmetry. $B_{17}H_{17}^{2-}$ also has high σ-aromaticity with four types of delocalized electrons ($3 \times 10\sigma_{delo}$ and $6\sigma_{delo}$).

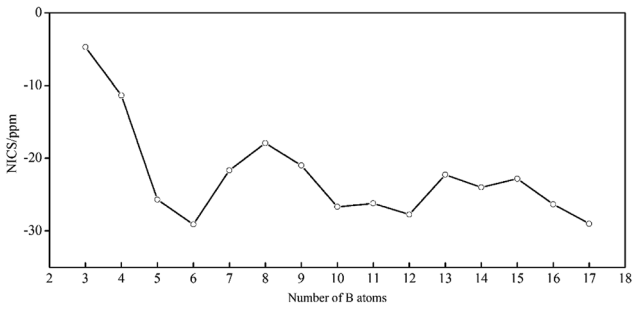

Fig. 9 Plot of Nucleus-Independent Chemical Shifts (NICS) for borane dianions $B_nH_n^{2-}$ ($n = 3$–17) (in ppm).

3.4 Flexibility of multicenter bonding

According to the bonding patterns of *closo*-$B_nH_n^{2-}$, their available topologic structures are exhibited in different lines and colors. As depicted in Fig. 10, there are different types of delocalized multicenter bonds, including open 3c–2e bond, close 3c–2e bond, 4c–2e bond, 8c–2e bond and fully delocalized bond, which

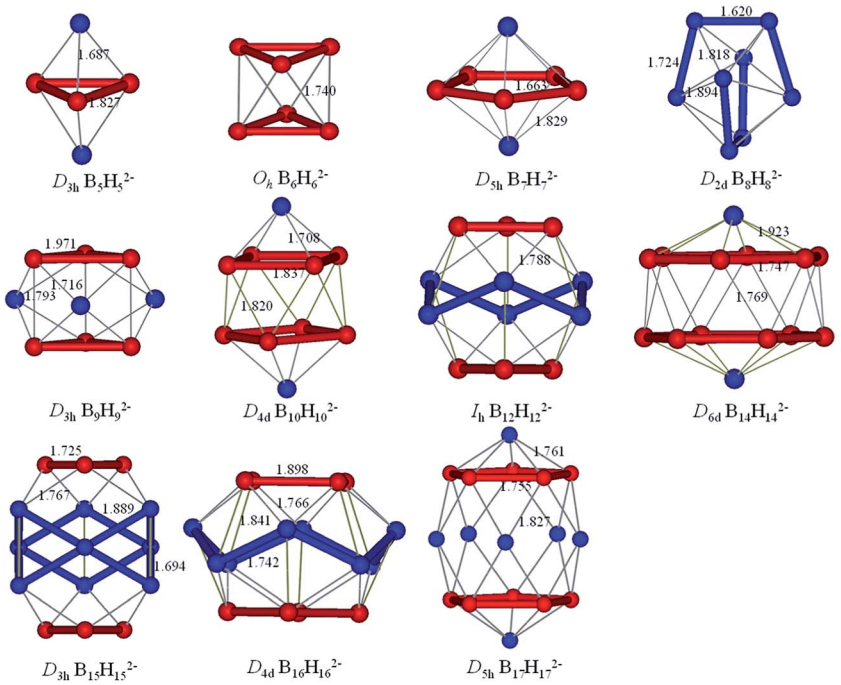

Fig. 10 Topology structures for *closo*-borane dianions, $B_nH_n^{2-}$ (n = 5–10, 12, 14–17).

corresponds to B_3 broken-line, B_3 triangle, B_4 rhombus, B_8 double-ring and the whole surface of boron cage in *closo*-$B_nH_n^{2-}$, respectively. The location of multicenter bond is related to the relative sizes of multi-membered rings and caps of clusters. In $B_{10}H_{10}^{2-}$, the 3c–2e bonds distribute on B_3 triangles of two caps at the top and bottom but of two multi-membered rings for $B_{14}H_{14}^{2-}$. Moreover, the bonding pattern of *closo*-$B_nH_n^{2-}$ are diversified both with their symmetry and with different B–B bond lengths. In $B_8H_8^{2-}$, $B_{12}H_{12}^{2-}$ and $B_{16}H_{16}^{2-}$, there are four, six and eight 3c–2e bonds on B_3 triangles, respectively, lying on the top and bottom, while the 4c–2e bonds distribute on B_4 rhombuses with longer B–B bond length. Thus, the flexibility of multicenter bonding can adapt well to all borane cages with different configurations. However, it is difficult to grasp clear generalizations of *closo*-borane clusters which is part of the attraction for study and distinct from carbon clusters.

4. Conclusion

The *closo*-borane dianion $B_nH_n^{2-}$ (n = 6–12) are proven to be stable and aromatic through the joint experimental and theoretical study. However, the bonding nature of *closo*-$B_nH_n^{2-}$ is still one of the mysteries in borane chemistry. In present work, we investigate the evolution rules of structures in $B_nH_n^{2-}$ (n = 2–17) and decipher their stability and aromaticity in the view of chemical bonding. $B_nH_n^{2-}$ with n = 2 and 3 are liner and planar structures, respectively, but undergo a transition between 2D and 3D structures at $B_4H_4^{2-}$. $B_nH_n^{2-}$ (n = 5–17) are inclined cage structures which have been explained by Wade's rules. There are ($4n$ + 2) valence electrons in $B_nH_n^{2-}$, the bonding in $B_2H_2^{2-}$ and $B_3H_3^{2-}$ are very similar to that in C_2H_2 and $C_3H_3^{+}$, respectively. Moreover, in *closo*-$B_nH_n^{2-}$, $2n$ valence electrons are involved in localized σ-BH bonds, the remaining ($2n$ + 2) valence electrons are evenly delocalized in either multicenter σ/π bonds, forming an effective σ and π delocalized system causing high stability, and σ/π aromaticity. The bonding in $B_5H_5^{2-}$ exits the 3c–2e open boron bridge bonds which was only observed in neutral borane preciously. For the high symmetry $B_6H_6^{2-}$ and $B_{12}H_{12}^{2-}$, one type of bonding patterns is given in a particular way in which any 3-fold axis has two delocalized valence electrons due to their resonance, while the other type of bonding patterns are listed in terms of superatom, both leading to high stability and aromaticity. In addition, we extend the concentric aromaticity of planar B_{13}^{+} to 3D $B_{15}H_{15}^{2-}$ and $B_{17}H_{17}^{2-}$ to explain their aromaticity. Moreover, it is found that the tendency of E_{HL} gaps in *closo*-$B_nH_n^{2-}$ are in accordance with their NICS values which indicates their close-shell electronic structures. In short, the highlight of our work is deciphering chemical bonding in *closo*-$B_nH_n^{2-}$, and the flexibility of multicenter bonding can adapt well to all borane cages with different configurations, making their stable and aromatic.

Acknowledgements

This work is financed by the National Natural Science Foundation of China (21573001), and by the Foundation of Distinguished Young Scientists of Anhui Province. The calculations were carried out at the High-Performance Computing Center of Anhui University.

References

1 R. Kawai and J. H. Weare, *J. Chem. Phys.*, 1991, **95**, 1151–1159.

2 I. Boustani, *Chem. Phys. Lett.*, 1995, **240**, 135–140.
3 A. Ricca and C. W. Bauschlicher Jr, *Chem. Phys.*, 1996, **208**, 233–242.
4 I. Boustani, *Phys. Rev. B*, 1997, **55**, 426–438.
5 E. Oger, N. R. Crawford, R. Kelting, P. Weis, M. M. Kappes and R. Ahlrichs, *Angew. Chem., Int. Ed.*, 2007, **46**, 8503–8506.
6 J. J. Zhao, L. Wang, F. Y. Li and Z. F. Chen, *J. Phys. Chem. A*, 2010, **114**, 9969–9972.
7 R. X. He and X. C. Zeng, *Chem. Commun.*, 2015, **51**, 3185–3188.
8 T. B. Tai and M. T. Nguyen, *Phys. Chem. Chem. Phys.*, 2015, **17**, 13672–13679.
9 T. B. Tai, L. V. Duong, H. T. Pham, D. T. Mai and M. T. Nguyen, *Chem. Commun.*, 2014, **50**, 1558–1560.
10 C. B. Kah, M. Yu, P. Tandy, C. S. Jayanthi and S. Y. Wu, *Nanotechnology*, 2015, **26**, 405701.
11 X. Y. Zhao, Q. Chen, H. R. Li, Y. W. Mu, H. G. Lu and S. D. Li, *Phys. Chem. Chem. Phys.*, 2017, **19**, 10998–11003.
12 Q. Chen, W. L. Li, Y. F. Zhao, S. Y. Zhang, H. S. Hu, H. Bai, H. R. Li, W. J. Tian, H. G. Lu, H. J. Zhai, S. D. Li, J. Li and L. S. Wang, *ACS Nano*, 2015, **9**, 754–760.
13 Q. Chen, S. Y. Zhang, H. Bai, W. J. Tian, T. Gao, H. R. Li, C. Q. Miao, Y. W. Mu, H. G. Lu, H. J. Zhai and S. D. Li, *Angew. Chem.*, 2015, **127**, 8278–8282.
14 Y. J. Wang, Y. F. Zhao, W. L. Li, T. Jian, Q. Chen, X. R. You, T. Ou, X. Y. Zhao, H. J. Zhai, S. D. Li, J. Li and L. S. Wang, *J. Chem. Phys.*, 2016, **144**, 064307.
15 T. B. Tai and M. T. Nguyen, *Nanoscale*, 2015, **7**, 3316–3317.
16 Z. A. Piazza, H. S. Hu, W. L. Li, Y. F. Zhao, J. Li and L. S. Wang, *Nat. Commun.*, 2014, **5**, 3113.
17 B. Feng, J. Zhang, Q. Zhong, W. Li, S. Li, H. Li, P. Cheng, S. Meng, L. Chen and K. Wu, *Nat. Chem.*, 2016, **8**, 563.
18 W. L. Li, Y. F. Zhao, H. S. Hu, J. Li and L. S. Wang, *Angew. Chem., Int. Ed.*, 2014, **53**, 5540–5545.
19 W. L. Li, Q. Chen, W. J. Tian, H. Bai, Y. F. Zhao, H. S. Hu, J. Li, H. J. Zhai, S. D. Li and L. S. Wang, *J. Am. Chem. Soc.*, 2014, **136**, 12257–12260.
20 A. P. Sergeeva, Z. A. Piazza, C. Romanescu, W. L. Li, A. I. Boldyrev and L. S. Wang, *J. Am. Chem. Soc.*, 2012, **134**, 18065–18073.
21 A. P. Sergeeva, D. Y. Zubarev, H. J. Zhai, A. I. Boldyrev and L. S. Wang, *J. Am. Chem. Soc.*, 2008, **130**, 7244–7246.
22 W. Huang, A. P. Sergeeva, H. J. Zhai, B. B. Averkiev, L. S. Wang and A. I. Boldyrev, *Nat. Chem.*, 2010, **2**, 202–206.
23 A. N. Alexandrova, A. I. Boldyrev, H. J. Zhai and L. S. Wang, *Coord. Chem. Rev.*, 2006, **250**, 2811–2866.
24 L. J. Cheng, *J. Chem. Phys.*, 2012, **136**, 104301.
25 I. A. Popov, T. Jian, G. V. Lopez, A. I. Boldyrev and L. S. Wang, *Nat. Commun.*, 2015, **6**, 8654.
26 D. Z. Li, H. Bai, T. Ou, Q. Chen, H. J. Zhai and S. D. Li, *J. Chem. Phys.*, 2015, **142**, 014302.
27 A. P. Sergeeva, I. A. Popov, Z. A. Piazza, W. L. Li, C. Romanescu, L. S. Wang and A. I. Boldyrev, *Acc. Chem. Res.*, 2014, **47**, 1349–1358.
28 B. Kiran, G. G. Kumar, M. T. Nguyen, A. K. Kandalam and P. Jena, *Inorg. Chem.*, 2009, **48**, 9965–9967.
29 T. B. Tai, D. J. Grant, M. T. Nguyen and D. A. Dixon, *J. Phys. Chem. A*, 2010, **114**, 994–1007.
30 B. Kiran, S. Bulusu, H. J. Zhai, S. Yoo, X. C. Zeng and L. S. Wang, *PNAS*, 2005, **102**, 961–964.
31 T. B. Tai, A. Ceulemans and M. T. Nguyen, *Chem.–Eur. J.*, 2012, **18**, 4510–4512.
32 M. P. Johansson, *J. Phys. Chem. C*, 2009, **113**, 524–530.
33 H. J. Zhai, Y. F. Zhao, W. L. Li, Q. Chen, H. Bai, H. S. Hu, Z. A. Piazza, W. J. Tian, H. G. Lu, Y. B. Wu, Y. W. Mu, G. F. Wei, Z. P. Liu, J. Li, S. D. Li and L. S. Wang, *Nat. Chem.*, 2014, **6**, 727–731.
34 S. D. Li, J. C. Guo, C. Q. Miao and G. M. Ren, *Angew. Chem., Int. Ed.*, 2005, **44**, 2158–2161.
35 C. Romanescu, T. R. Galeev, W. L. Li, A. I. Boldyrev and L. S. Wang, *Angew. Chem., Int. Ed.*, 2011, **50**, 9334–9337.
36 B. P. Fokwa and M. Hermus, *Angew. Chem., Int. Ed.*, 2012, **51**, 1702–1705.
37 Y. Yuan and L. J. Cheng, *J. Chem. Phys.*, 2013, **138**, 024301.
38 L. F. Li, C. Xu, B. K. Jin and L. J. Cheng, *Dalton Trans.*, 2014, **43**, 11739–11744.
39 M. Mbarki, R. St Touzani and B. P. Fokwa, *Angew. Chem., Int. Ed.*, 2014, **53**, 13174–13177.
40 B. Mondal, B. Mondal, K. Pal, B. Varghese and S. Ghosh, *Chem. Commun.*, 2015, **51**, 3828–3831.
41 H. J. Zhai, A. N. Alexandrova, K. A. Birch, A. I. Boldyrev and L. S. Wang, *Angew. Chem., Int. Ed.*, 2003, **42**, 6004–6008.
42 C. Romanescu, T. R. Galeev, W. L. Li, A. I. Boldyrev and L. S. Wang, *J. Chem. Phys.*, 2013, **138**, 134315.
43 S. Li, Z. Zhang, Z. Long and S. Qin, *Sci. Rep.*, 2017, **7**, 40081.
44 Q. Chen, H. R. Li, C. Q. Miao, Y. J. Wang, H. G. Lu, Y. W. Mu, G. M. Ren, H. J. Zhai and S. D. Li, *Phys. Chem. Chem. Phys.*, 2016, **18**, 11610–11615.
45 H. Bai, Q. Chen, H. J. Zhai and S. D. Li, *Angew. Chem., Int. Ed.*, 2015, **54**, 941–945.
46 Q. Chen, T. Gao, W. J. Tian, H. Bai, S. Y. Zhang, H. R. Li, C. Q. Miao, Y. W. Mu, H. G. Lu, H. J. Zhai and S. D. Li, *Phys. Chem. Chem. Phys.*, 2015, **17**, 19690–19694.
47 W. L. Li, T. Jian, X. Chen, H. R. Li, T. T. Chen, X. M. Luo, S. D. Li, J. Li and L. S. Wang, *Chem. Commun.*, 2017, **53**, 1587–1590.
48 W. L. Li, C. Romanescu, T. R. Galeev, Z. A. Piazza, A. I. Boldyrev and L. S. Wang, *J. Am. Chem. Soc.*, 2012, **134**, 165–168.
49 W. J. Tian, Q. Chen, X. X. Tian, Y. W. Mu, H. G. Lu and S. D. Li, *Sci. Rep.*, 2016, **6**, 8.
50 W. N. Lipscomb, *Boron Hydrides*, ed. W. A. Benjamin, New York, 1963.
51 M. F. Hawthorne and A. R. Pitochelli, *J. Am. Chem. Soc.*, 1959, **81**, 5519.
52 A. R. Pitochelli and F. M. Hawthorne, *J. Am. Chem. Soc.*, 1960, **82**, 3228–3229.
53 J. L. Boone, *J. Am. Chem. Soc.*, 1964, **86**, 5036.
54 F. Klanberg and E. Muetterties, *Inorg. Chem.*, 1966, **5**, 1955–1960.
55 F. Klanberg, D. R. Eaton, L. J. Guggenberger and E. L. Muetterties, *Inorg. Chem.*, 1967, **6**, 1271–1281.

56 F. Schluter and E. Bernhardt, *Inorg. Chem.*, 2011, **50**, 2580–2589.
57 N. Zint, A. Dreuw and L. S. Cederbaum, *J. Am. Chem. Soc.*, 2002, **124**, 4910–4917.
58 L. D. Brown and W. N. Lipscomb, *Inorg. Chem.*, 1977, **16**, 2989–2996.
59 K. Wade, *J. Chem. Soc. D*, 1971, **549**, 792–793.
60 D. M. P. Mingos, *Nature (London), Phys. Sci.*, 1972, **236**, 99–102.
61 D. M. P. Mingos, *Acc. Chem. Res.*, 1984, **17**, 311–319.
62 R. B. King and D. H. Rouvray, *J. Am. Chem. Soc.*, 1977, **9**, 7834–7840.
63 M. E. O'Neill and K. Wade, *THEOCHEM*, 1983, **103**, 259–268.
64 M. E. O'Neill and K. Wade, *Polyhedron*, 1984, **3**, 199–212.
65 S. Mebs, R. Kalinowski, S. Grabowsky, D. Forster, R. Kickbusch, E. Justus, W. Morgenroth, C. Paulmann, P. Luger, D. Gabel and D. Lentz, *Inorg. Chem.*, 2011, **50**, 90–103.
66 Y. Yuan and L. J. Cheng, *J. Chem. Phys.*, 2012, **137**, 044308.
67 L. F. Li, C. Xu and L. J. Cheng, *Comput. Theor. Chem.*, 2013, **1021**, 144–148.
68 L. F. Li, C. Xu, B. K. Jin and L. J. Cheng, *J. Chem. Phys.*, 2013, **139**, 174310.
69 J. Tao, J. P. Perdew, V. N. Staroverov and G. E. Scuseria, *Phys. Rev. Lett.*, 2003, **91**, 146401.
70 C. Xu, L. J. Cheng and J. L. Yang, *J. Chem. Phys.*, 2014, **141**, 124301.
71 P. v. R. Schleyer, C. Maerker, A. Dransfeld, H. Jiao and N. J. R. v. E. Hommes, *J. Am. Chem. Soc.*, 1996, **118**, 6317–6318.
72 M. Frisch, G. Trucks, H. B. Schlegel, G. Scuseria, M. Robb, J. Cheeseman, G. Scalmani, V. Barone, B. Mennucci and G. Petersson, *Gaussian 09, Revision B. 01*, Gaussian Inc., Wallingford, CT, 2010.
73 D. Y. Zubarev and A. I. Boldyrev, *Phys. Chem. Chem. Phys.*, 2008, **10**, 5207–5217.
74 W. L. Li, T. Jian, X. Chen, T. T. Chen, G. V. Lopez, J. Li and L. S. Wang, *Angew. Chem.*, 2016, **128**, 7484–7489.
75 E. Osorio, J. K. Olson, W. Tiznado and A. I. Boldyrev, *Chem.–Eur. J.*, 2012, **18**, 9677–9681.
76 A. P. Sergeeva, B. B. Averkiev, H. J. Zhai, A. I. Boldyrev and L. S. Wang, *J. Chem. Phys.*, 2011, **134**, 224304.
77 E. R. Johnson, S. Keinan, P. Mori-Sanchez, J. Contreras-Garcia, A. J. Cohen and W. Yang, *J. Am. Chem. Soc.*, 2010, **132**, 6498–6506.
78 T. Lu and F. Chen, *J. Comput. Chem.*, 2012, **33**, 580–592.
79 W. Humphrey, A. Dalke and K. Schulten, *J. Mol. Graphics*, 1996, **14**, 33–38.
80 U. Varetto, *Molekel 5.4.0.8*, Swiss National Supercomputing Centre, Manno, Switzerland.
81 P. v. R. Schleyer, K. Najafian and A. M. Mebel, *Inorg. Chem.*, 1998, **37**, 6765–6772.
82 A. Dreuw, N. Zint and L. S. Cederbaum, *J. Am. Chem. Soc.*, 2002, **124**, 10903–10910.
83 R. Schaeffer, Q. Johnson and G. S. Smith, *Inorg. Chem.*, 1965, **4**, 917–918.
84 J. F. Jia, L. J. Ma, J. F. Wang and H. S. Wu, *J. Mol. Model.*, 2013, **19**, 3255–3261.
85 D. T. Mai, L. V. Duong, T. B. Tai and M. T. Nguyen, *J. Phys. Chem. A*, 2016, **120**, 3623–3633.
86 A. J. Welch, *Chem. Commun.*, 2013, **49**, 3615–3616.
87 D. Y. Zubarev and A. I. Boldyrev, *J. Org. Chem.*, 2008, **73**, 9251–9258.
88 B. K. Teo, *J. Cluster Sci.*, 2014, **25**, 883–891.
89 W. S. Hopkins, P. J. Carr, D. Huang, K. P. Bishop, M. Burt, T. B. McMahon, V. Steinmetz and E. Fillion, *J. Phys. Chem. A*, 2015, **119**, 8469–8475.
90 G. S. Nevill and C. J. Tymczak, *Nanoscale Res. Lett.*, 2012, **7**, 236.
91 W. Huang, A. P. Sergeeva, H. J. Zhai, B. B. Averkiev, L. S. Wang and A. I. Boldyrev, *Nat. Chem.*, 2010, **2**, 202–206.
92 J. Poater, M. Sola, C. Vinas and F. Teixidor, *Chem.–Eur. J.*, 2016, **22**, 7437–7443.